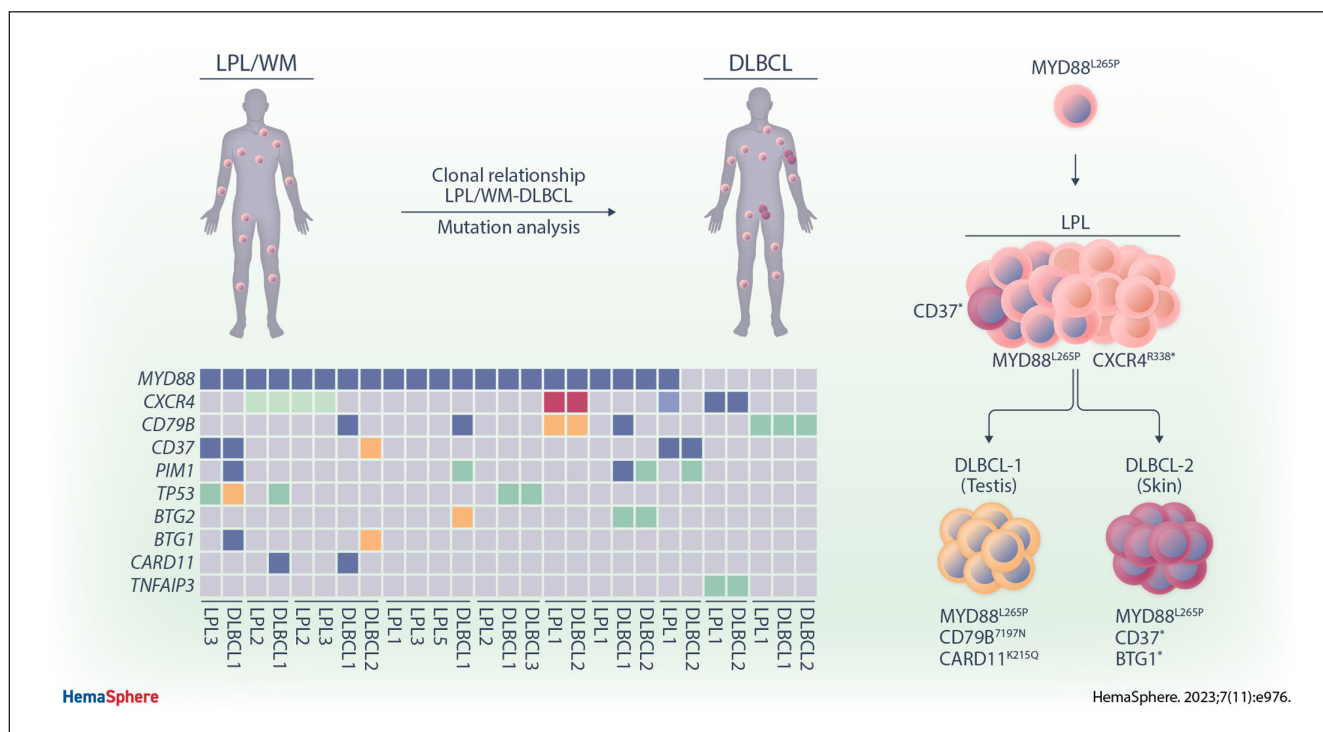


Article
Open Access

Clonal Relationship and Mutation Analysis in Lymphoplasmacytic Lymphoma/Waldenström Macroglobulinemia Associated With Diffuse Large B-cell Lymphoma

Madeleine R. Berendsen¹, Diede A.G. van Bladel¹, Eva Hesius², Cristina Berganza Irusquieta¹, Jos Rijntjes¹, Annemiek B. van Spriel³, Ellen van der Spek⁴, Johannes F.M. Pruijt⁵, Leonie I. Kroeze¹, Konnie M. Hebeda¹, Sandra Croockewit², Wendy B.C. Stevens², J Han J.M. van Krieken¹, Patricia J.T.A. Groenen¹, Michiel van den Brand⁶, Blanca Scheijen¹


GRAPHICAL ABSTRACT



Article

Open Access

Clonal Relationship and Mutation Analysis in Lymphoplasmacytic Lymphoma/Waldenström Macroglobulinemia Associated With Diffuse Large B-cell Lymphoma

Madeleine R. Berendsen¹, Diede A.G. van Bladel¹, Eva Hesius², Cristina Berganza Iruquieta¹, Jos Rijntjes¹, Annemiek B. van Spruiel³, Ellen van der Spek⁴, Johannes F.M. Pruijt⁵, Leonie I. Kroeze¹, Konnie M. Hebeda¹, Sandra Croockewit², Wendy B.C. Stevens², J Han J.M. van Krieken¹, Patricia J.T.A. Groenen¹, Michiel van den Brand⁶, Blanca Scheijen¹ 

Correspondence: Blanca Scheijen (blanca.scheijen@radboudumc.nl).

ABSTRACT

Patients with lymphoplasmacytic lymphoma/Waldenström macroglobulinemia (LPL/WM) occasionally develop diffuse large B-cell lymphoma (DLBCL). This mostly results from LPL/WM transformation, although clonally unrelated DLBCL can also arise. LPL/WM is characterized by activating *MYD88*^{L265P} (>95%) and *CXCR4* mutations (~30%), but the genetic drivers of transformation remain to be identified. Here, in thirteen LPL/WM patients who developed DLBCL, the clonal relationship of LPL and DLBCL together with mutations contributing to transformation were investigated. In 2 LPL/WM patients (15%), high-throughput sequencing of immunoglobulin gene rearrangements showed evidence of >1 clonal B-cell population in LPL tissue biopsies. In the majority of LPL/WM patients, DLBCL presentations were clonally related to the dominant clone in LPL, providing evidence of transformation. However, in 3 patients (23%), DLBCL was clonally unrelated to the major malignant B-cell clone in LPL, of which 2 patients developed de novo DLBCL. In this study cohort, LPL displayed *MYD88*^{L265P} mutation in 8 out of eleven patients analyzed (73%), while *CXCR4* mutations were observed in 6 cases (55%). *MYD88*^{WT} LPL biopsies present in 3 patients (27%) were characterized by *CD79B* and *TNFAIP3* mutations. Upon transformation, DLBCL acquired novel mutations targeting *BTG1*, *BTG2*, *CD79B*, *CARD11*, *TP53*, and *PIM1*. Together, we demonstrate variable clonal B-cell dynamics in LPL/WM patients developing DLBCL, and the occurrence of clonally unrelated DLBCL in about one-quarter of LPL/WM patients. Moreover, we identified commonly mutated genes upon DLBCL transformation, which together with preserved mutations already present in LPL characterize the mutational landscape of DLBCL occurrences in LPL/WM patients.

INTRODUCTION

Lymphoplasmacytic lymphoma (LPL) is an incurable B-cell neoplasm composed of a spectrum of small B lymphocytes,

lymphoplasmacytoid cells, and plasma cells. The majority of LPL patients (>90%) are clinically diagnosed with Waldenström macroglobulinemia (WM), characterized by bone marrow (BM) infiltration of clonal lymphoplasmacytic cells and serum monoclonal immunoglobulin M (IgM) paraprotein.^{1,2} LPL/WM is a heterogeneous disease and mostly follows an indolent clinical course with a median survival of 10 years. However, in 2%–10% of LPL/WM patients development of diffuse large B-cell lymphoma (DLBCL) is observed, often resulting from LPL transformation, and associated with a poor prognosis.^{3–6} Here, different models of clonal evolution have been proposed, including linear and divergent clonal evolution.^{7,8} DLBCL presentations in antecedent LPL/WM are often localized at extranodal sites, frequently with an activated B-cell phenotype.^{5,6} Extranodal DLBCL includes cutaneous involvement, and lymphomas located at immune-privileged (IP) sites, such as central nervous system (CNS) and testis. Besides transformation, the occurrence of clonally unrelated DLBCL has been reported in LPL/WM.^{7–11} Clonotypic V(D)J analysis has also demonstrated biclonality in a subset of LPL/WM,^{12–14} but it is still unclear whether these patients are at increased risk of DLBCL development.

The molecular hallmark of LPL/WM is the activating p.L265P hotspot mutation in the *MYD88* (*MYD88*^{L265P}) gene in

¹Department of Pathology, Radboud University Medical Center, Nijmegen, The Netherlands

²Department of Hematology, Radboud University Medical Center, Nijmegen, The Netherlands

³Department of Medical BioSciences, Radboud University Medical Center, Nijmegen, The Netherlands

⁴Department of Hematology, Rijnstate Hospital, Arnhem, The Netherlands

⁵Department of Hematology, Jeroen Bosch Hospital, 's-Hertogenbosch, The Netherlands

⁶Pathology-DNA, Rijnstate Hospital, Arnhem, The Netherlands

Supplemental digital content is available for this article. Copyright © 2023 the Author(s). Published by Wolters Kluwer Health, Inc. on behalf of the European Hematology Association. This is an open-access article distributed under the terms of the Creative Commons Attribution-Non Commercial-No Derivatives License 4.0 (CCBY-NC-ND), where it is permissible to download and share the work provided it is properly cited. The work cannot be changed in any way or used commercially without permission from the journal. *HemaSphere* (2023) 7:11(e976).

<http://dx.doi.org/10.1097/HS9.0000000000000976>.

Received: June 27, 2023 / Accepted: September 21, 2023

>95% of the patients,^{15–18} which triggers anti-apoptotic NF- κ B signaling enabling cell survival during B-cell development. LPL/WM patients with wild-type *MYD88* gene (*MYD88*^{WT}) show a shorter survival with a higher incidence of DLBCL-associated events.^{19,20} The *CXCR4* gene, encoding the chemokine receptor of ligand CXCL12, is the second most common target for mutations in LPL/WM, and *CXCR4* mutations (*CXCR4*^{MUT}) are detected in ~30% of patients.^{21–23} The majority of *CXCR4* mutations introduce a premature stop codon within the regulatory cytosolic domain that impairs receptor internalization, thereby prolonging signaling and downstream activation of AKT and MAPK upon binding to CXCL12.²³ *CXCR4*^{MUT} patients show a more aggressive disease at diagnosis.^{22,23} Other recurrently affected genes in LPL/WM involve *KMT2D*, *ARID1A*, *CD79B*, and *TP53*,^{21,24} but the genetic alterations driving transformation remain to be identified.

Here, we describe the clonal relationship and B-cell dynamics of LPL and DLBCL presentations within the same patient, which was investigated by next-generation sequencing (NGS)-based detection of immunoglobulin heavy chain (IGH) and kappa light chain (IGK) gene rearrangements. This represents a sensitive assay to detect small clonal B-cell populations, as demonstrated recently with clonality assessment in classic Hodgkin lymphoma tissue specimens.²⁵ In addition, targeted mutation analysis was performed in paired LPL and DLBCL tissue samples to determine which mutations contributed to the transformation.

MATERIALS AND METHODS

LPL/WM patient cohort

The study cohort consisted of 13 patients from whom LPL and DLBCL tissue biopsies were available with clinically confirmed LPL/WM and DLBCL diagnoses. Archival material from 1997 to 2019 was obtained from the Pathology departments of Radboud University Medical Center (Nijmegen, the Netherlands), Rijnstate Hospital (Arnhem, the Netherlands), and Jeroen Bosch Hospital (*s-Hertogenbosch, the Netherlands). All LPL and DLBCL tissue biopsies were reviewed by experienced hematopathologists according to the 2022 World Health Organization classification. Clinical and pathological information is summarized in Suppl. Table S1. Monoclonal IgM paraprotein was detected in 8 patients confirming WM diagnosis, and for uniformity, all LPL/WM tissue biopsies were described as LPL in our study descriptions. All samples and clinical information were collected in accordance with the Declaration of Helsinki and the Declaration of Taipei and received approval from the local medical ethical review board (CMO Approval Number: 2020-6390).

Immunohistology

DLBCL biopsies were fixed in formalin, while LPL bone marrow biopsies were fixed in either Burkhardt or formalin and decalcified with EDTA. For uniformity, we describe both tissue sources as formalin-fixed and paraffin-embedded (FFPE) tissues in the study descriptions. Tissue slides (4 μ m) were stained with hematoxylin and eosin and with monoclonal antibodies directed against human CD20 (clone L26; Thermo Fisher Scientific, Waltham, MA), CD79a (clone JCB117, DAKO; Agilent Technologies Inc., Carpinteria, CA), IGKs (DAKO, Agilent Technologies Inc.), Lambda light chains (DAKO; Agilent Technologies Inc.), and CD138 (clone B-A38; Thermo Fisher Scientific).

Next-generation sequencing-based detection of immunoglobulin gene rearrangements

NGS-based clonality analysis was performed on genomic DNA isolated from FFPE tumor tissues using approximately

8 tissue sections of 10 μ m, and the QIAamp DNA FFPE Tissue Kit (Qiagen, Hilden Germany). DNA concentrations were determined using Qubit (dsDNA BR Assay Kit; Life Technologies, Carlsbad, CA). NGS-based clonality analysis was performed as previously described by the EuroClonality-NGS Working Group to detect productive and unproductive IGH and IGK gene rearrangements.^{26–28} The 4 standard targets of the EuroClonality IG-NGS assay (framework-3 [FR3] IGHV-IGHD-IGHJ, IGHD-IGHJ, IGKV-IGKJ, and IGKV/Intron RSS-KDE) were analyzed for all LPL and DLBCL samples using 40 ng DNA input (or a minimum of 10 ng for samples with limited material available) for each of the 3 multiplex PCR reactions with M13-tailed primers. Library preparations were generated in a second step with adaptor-tailed M13 primers compatible with sequencing on an Illumina platform. Samples were pooled at equal molarity (4 nM) loaded on an Illumina mid-output chip and sequenced with MiniSeq500. NGS datasets were analyzed using the bioinformatics analysis tool ARResT/Interrogate (<http://arrest.tools/interrogate>). Guidelines for molecular scoring of IG clonality assessment in DLBCL have been described previously.²⁹ For this study cohort, the identification of clonal gene rearrangements corresponding to lymphoma-associated clonotypes was defined by the following threshold criteria: a ≥ 3.2 fold higher abundance compared to background clonotypes for IGHV-IGHD-IGHJ (FR3) target, ≥ 5.7 fold for IGHD-IGHJ, ≥ 5.8 fold for IGKV-IGKJ, and ≥ 7.6 fold for both IGKV-KDE and Intron RSS-KDE, which were combined in clonotype analysis. Clonotypes corresponding to non-malignant background B-cells were determined as the average percentage of clonotypes 3 to 7 identified by the Arrest/Interrogate analysis pipeline, or the next ranked clonotypes in case of >2 dominant B-cell clones. B-cell clonality was classified as (1) no clonal product in case of <1000 reads due to the inability to detect a clonal IG rearrangement, non-reproducibility after technical replicate analysis or an ambiguous pattern; (2) polyclonal in samples with sufficient reads and multiple clonotypes representing background B-cells without the presence of a dominant B-cell clone; (3) clonal corresponding to a major B-cell clone fulfilling all threshold criteria, or a minor B-cell clone detected in top-15 of the most frequent clonotypes and present as a major dominant clone in a paired sample in the same patient.

Targeted mutation analysis with smMIP assay

Mutation analyses were performed using single molecule molecular inversion probes (smMIPs) targeting defined exonic regions of a dedicated panel of 11 target genes (Suppl. Table S2). An automated workflow for smMIP pool and library preparation was performed as described previously.³⁰ For each sample 100 ng input DNA was used and sequencing was performed on the Illumina NovaSeq platform using paired-end sequencing. NGS data output was analyzed with SeqNext software (JSI Medical Systems), in which a minimum coverage of $n = 20$ reads was required for each MIP. PCR duplicates were eliminated by consensus clustering of reads through the identification of a unique molecular identifier (UMI), while FFPE artifacts were excluded by eliminating single-strand-oriented cytosine deamination variants. Solely variants with a minimum of $n = 5$ combined mutant reads and a minimum variant allele frequency (VAF) of 5% were included. For mutational calling, synonymous variants, intronic variants (with the exception of splice sites), and germline variants were excluded. Several germline databases were applied and variants were only included in cases <0.1% in EXAC AF, <0.05% in Gnomad-G-AF, and <0.1% prevalence in the in-house germline database. All identified mutations were checked for their presence in the corresponding paired LPL and DLBCL samples.

RESULTS

Clinicopathological characteristics of LPL/WM patient cohort with DLBCL occurrences

In this study cohort, paired biopsies of thirteen LPL/WM patients who were also diagnosed with DLBCL at any given timepoint were included for analysis. The median age of LPL/WM diagnosis was 58 years (range 41–72 years), and most of these patients received chlorambucil-including chemotherapeutic regimens when presented with symptomatic disease (Table 1; Suppl. Table S1). The median age at first DLBCL diagnosis was 65 years (range 49–78 years), which involved stage IV DLBCL disease in 50% of patients, and high-intermediate IPI score in 36% of patients. Upon primary DLBCL diagnosis, all patients were treated with (immuno-)chemotherapy and 5-year overall survival was 38%. In most patients ($n = 11/13$; 85%), LPL biopsies were available preceding the diagnosis of the first DLBCL (interval range first available LPL biopsy-DLBCL diagnosis: 0.8–18.7 years), some of which involved a biopsy of first LPL diagnosis. In 8 patients, sequential LPL biopsies (before or after DLBCL) were available for molecular analysis. From another set of 8 patients >1 DLBCL biopsy was included for analysis, which involved either biopsies from different anatomical locations taken at the same timepoint, or subsequent relapsed sample(s). In total, 28 LPL tissue specimens were subjected to molecular analysis, which involved biopsies from different anatomical sites, including BM ($n = 22$), orbit ($n = 2$), retroperitoneum ($n = 1$), lymph node ($n = 1$) and spleen ($n = 2$). DLBCL biopsies ($n = 23$) were available from 4 nodal (17%) and 19 extranodal sites (83%), of which 7 were IP-DLBCL. These included DLBCL, not otherwise specified located in the testis ($n = 5$) or CNS ($n = 2$).

Table 1

Clinicopathological Data of LPL/WM Cohort

Gender, $n = 13$	
Female	2 (15%)
Male	11 (85%)
Age at DLBCL diagnosis, $n = 13$	
<60	3 (23%)
≥60	10 (77%)
Stage DLBCL, $n = 12$	
I	4 (33%)
II	1 (8%)
III	1 (8%)
IV	6 (50%)
IPI DLBCL, $n = 11$	
Low	4 (36%)
Low-intermediate	3 (27%)
High-intermediate	4 (36%)
High	0 (0%)
First-Line DLBCL treatment, $n = 13$	
Immuno-chemotherapy	12 (92%)
Chemotherapy	1 (8%)
Site of DLBCL biopsy diagnosis, $n = 13$	
Nodal	3 (23%)
Extranodal	10 (77%)
Immune-privileged	6 (46%)
Included DLBCL relapses, $n = 13$	
0	7 (54%)
1	6 (46%)
Interval LPL biopsy preceding DLBCL	
Interval	0.8–18.7 y
LPL treatments, $n = 13$	
Chlorambucil included	9 (69%)

In the case of nodal and extranodal biopsy, only nodal is indicated here. Immuno indicates rituximab treatment. (Immuno-)chemotherapy was combined with radiotherapy in a proportion of patients. DLBCL = diffuse large B-cell lymphoma; IP= immune-privileged; LPL = lymphoplasmacytic lymphoma; LPL/WM = lymphoplasmacytic lymphoma/ Waldenström macroglobulinemia.

Temporal and spatial clonal B-cell dynamics in LPL tissue specimens

The clonal B-cell composition in LPL tissue biopsies was assessed by NGS-based clonality assays as developed by the Euroclonality-NGS Working Group.^{26–28} IG-NGS clonality analysis detected clonal B-cells in all but 2 LPL tissue samples (due to inferior genomic DNA quality), based on the presence of clonal IG gene rearrangements at either the IGH loci ($n = 3/26$; 12%) or a combination of IGH and IGK loci ($n = 23/26$; 88%) (Suppl. Table S3). No obviously biased IGHV and IGKV gene usage was observed. Two patterns of clonal LPL dynamics could be identified by IG-NGS in LPL preceding DLBCL diagnosis ($n = 11$): (1) clonal expansion of 1 B-cell clone ($n = 9$), which remained stably present for a given time period before DLBCL occurrence, even up to ~19 years after the initial LPL/WM diagnosis (case 2) (Figure 1); (2) clonal expansion of >1 B-cell population in LPL biopsies at different stages of the disease ($n = 2$; case 4, case 5), including a biclonal LPL that progressed over time to a clonal LPL (case 5) (Figure 2). In 2 patients, LPL biopsies were only available after DLBCL diagnosis, and these reflected single clonal B-cell expansions (case 7 and case 13). Together, our data reveal that in this study cohort, 2 out of 13 LPL/WM patients with DLBCL presentations (15%) showed evidence of multiple malignant B-cell clones in LPL tissue biopsies.

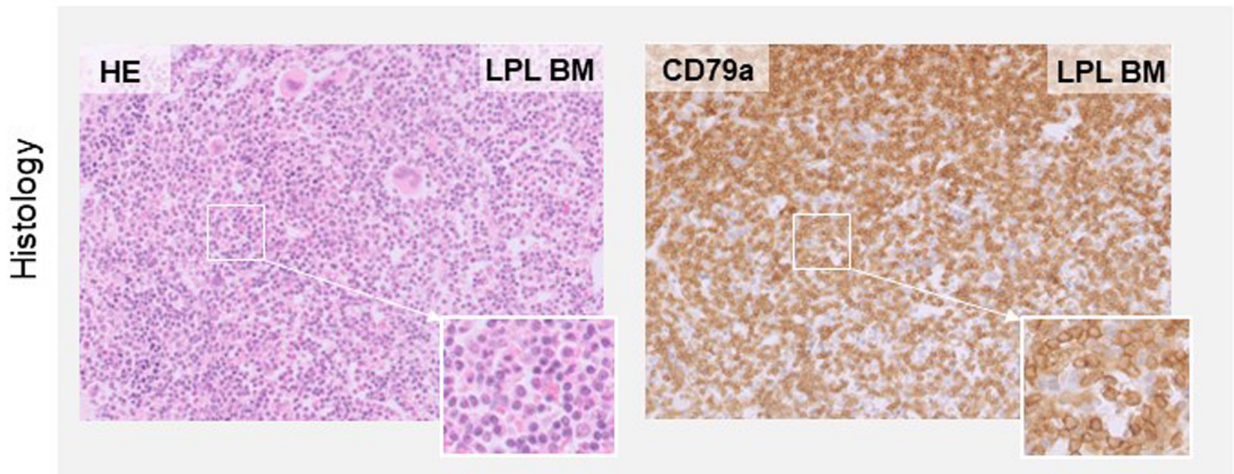
Besides this pattern of temporal clonal dynamics, in one of these patients (case 4) a distinct spatial profile was observed by IG-NGS (Figure 3; Suppl Figure S1; Suppl. Table S4). Two independent synchronous LPL biopsies of orbit and BM displayed a distinct pattern of clonal IG rearrangements. The dominant IGH (IGHV3-72 -2/25/0 J4) and IGK (IGKV1-9 -3/1/-1 J4) clonotypes of clonal B-cells observed in BM represented only a minor subclone in the orbital LPL biopsy. The other more dominant IGH (IGHV4-59 -0/22/-1 J1; IGHD2-2 -4/60/-5 J4) and IGK (IGKV3-20 -1/1/-4 Kde; IGKV1-16 -0/0/-0 Kde) clonotypes in the orbital LPL biopsy were not present as clonal B-cells in BM. Thus, variable and distinct clonal B-cell populations were present at different anatomical sites in this patient. LPL biopsies at different anatomical locations in 2 other patients (spleen and BM of case 6, retroperitoneum and BM of case 7) showed identical dominant clonotypes in each of these sites.

Clonal relationship of LPL and DLBCL occurrences

B-cell clonality analysis with EuroClonality BIOMED-2/ GeneScan assays,^{31–33} and more recently by IG-NGS^{27,29} has demonstrated detection of clonal IG gene rearrangements in ~80% of DLBCL cases. In this study cohort, all DLBCL samples showed clonal IG gene rearrangements with NGS at either IGH loci ($n = 3/23$; 13%) or a combination of IGH and IGK loci ($n = 20/23$; 87%). From the 8 LPL/WM patients with multiple DLBCL tissue biopsies, clonal IG gene rearrangements were identical between the different DLBCL samples of the same patient, except for 1 patient (case 7) where the dominant clonotypes of the extranodal DLBCL in the orbit (IGHV3-33 -0/25/-5 J4; IGKV4-1 -8/6/-2 J2; DLBCL-2) were distinct from the testicular DLBCL (IGHV3 -0/10/-17 J4; IGKV1-5 = IGKV1-17 -8/3/-7 J1; DLBCL-1) (Suppl. Table S3).

Next, clonal comparison of the identified dominant clonotypes between the paired LPL and DLBCL samples was performed for the total cohort of LPL/WM patients ($n = 13$). Clonally related DLBCL (including DLBCL-1 of case 7) was detected in 11 out of 13 LPL/WM patients (85%), where the clonal IG gene rearrangements in LPL were identical to the DLBCL biopsies for most of the targets, indicating the histological transformation of LPL to DLBCL. In the majority of cases ($n = 10$), the dominant B-cell clone residing in the (consecutive) LPL biopsies represented the major B-cell clone in DLBCL (Figure 4A). However, in 1 patient the B-cell clone giving rise to DLBCL transformation represented a minor clone in the first BM LPL biopsy but dominated in LPL at later timepoints (case 5). In 3 cases of paired clonally related LPL and DLBCL

A



B

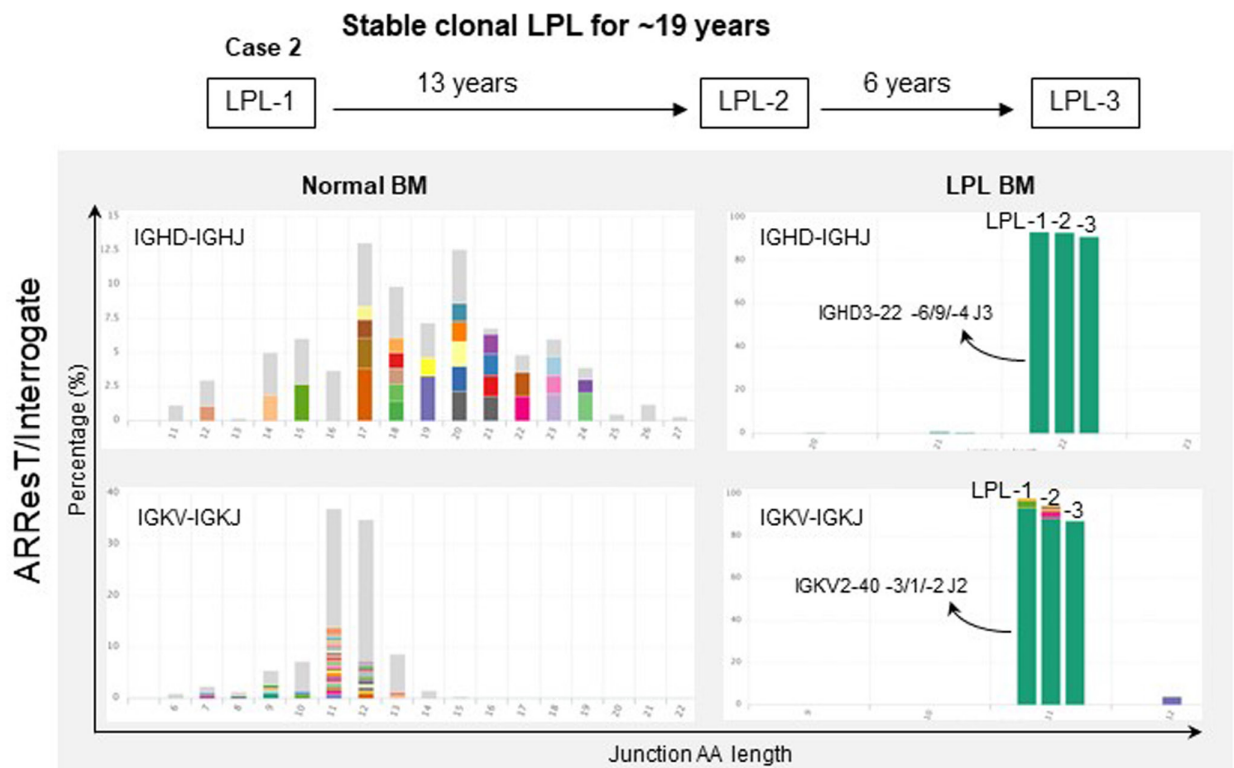


Figure 1. Histology and NGS-based clonality analysis of LPL bone marrow biopsies with stable clonal disease. (A) Representative section of an LPL bone marrow (BM) biopsy (case 2) stained with hematoxylin and eosin (H&E) (left panel), or CD79a antibody (right panel). Images were taken at 200x magnification, and the insert shows a zoom-in. (B) Next-generation sequencing (NGS)-based clonality assessment combined with ARResT/Interrogate bioinformatics reveals the distribution of clonotypes as detected by the analysis of IGHD-IGHJ and IGKV-IGKJ gene rearrangements in normal BM (left panels), and consecutive LPL biopsies (LPL-1, LPL-2, LPL-3) of case 2 (right panels) with stable clonal expansion over a period of ~19 years. The relative abundance of each clonotype per indicated target is depicted on the y-axis and the junction amino acid (AA) length on the x-axis. The most dominant clonotype is indicated in green, and the identity of the dominant clonotype is shown. A clonotype is defined by the 5' and 3' gene annotation and the junctional nucleotide sequence of the rearrangement. AA = amino acid; BM = bone marrow; HE = hematoxylin and eosin; LPL = lymphoplasmacytic lymphoma; NGS = next-generation sequencing.

biopsies, a few nucleotide differences were observed between consecutive samples (Suppl. Table S5), indicative of ongoing somatic hypermutation (SHM) between LPL and DLBCL presentations, which resulted in minor differences with respect to the clonotype annotation.

Besides the clonally related DLBCL tissue biopsies, DLBCL presentations of 3 patients (23%, case 4, case 7, case 13) showed different clonal IG gene rearrangements as compared to

the dominant B-cell clone in LPL, indicating clonally unrelated DLBCL (Figure 5). In 1 patient (case 7), this was the case for the orbital DLBCL (DLBCL-2), but not the testicular DLBCL (DLBCL-1), showing distinct IGHD-IGHJ and IGKV-IGKJ gene rearrangements (Figure 4B). The clonotypes corresponding to the malignant B-cell clone of the clonally unrelated orbital DLBCL were non-detectable by IG-NGS in any of the LPL samples (n = 2; case 7). In another patient (case 13), the

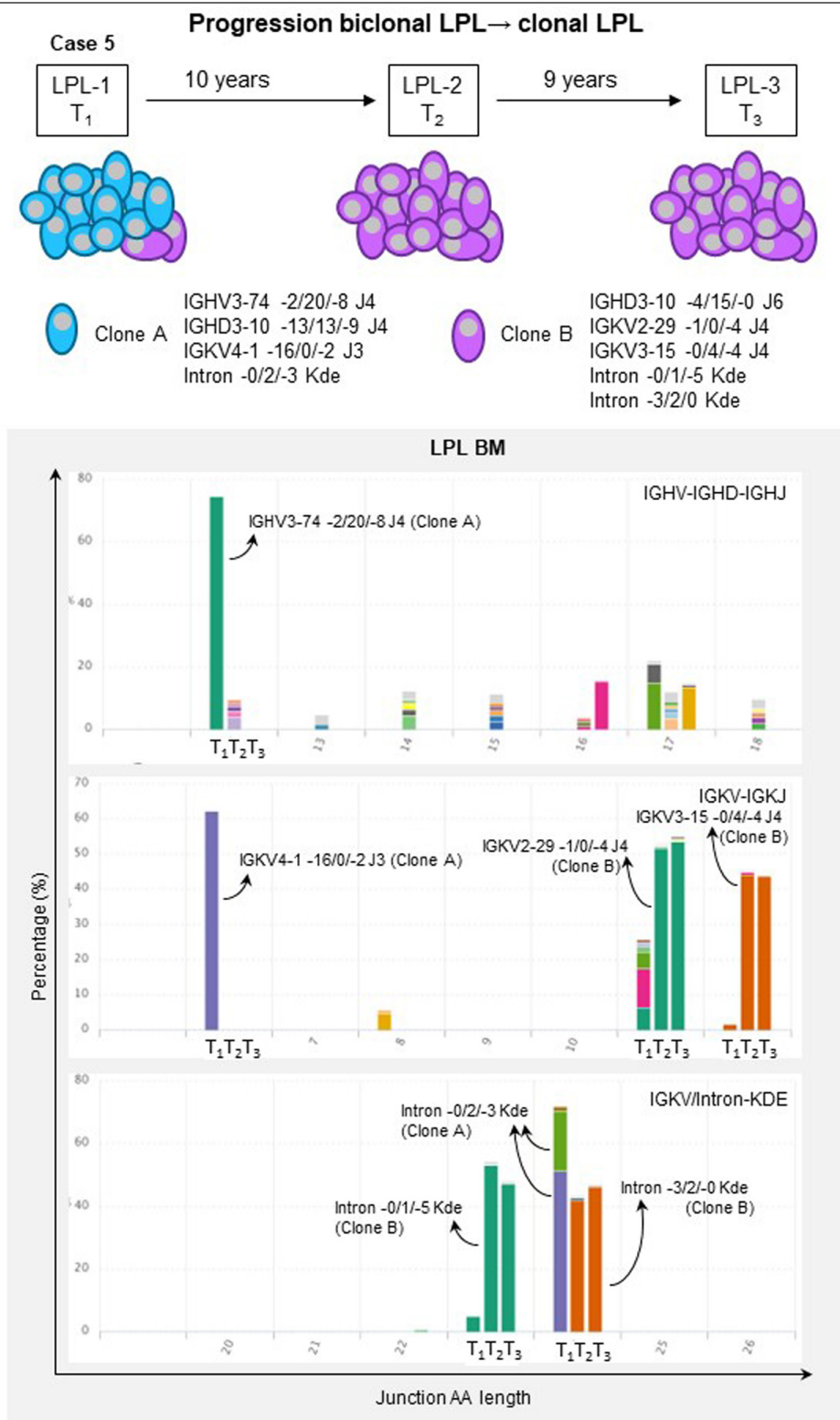
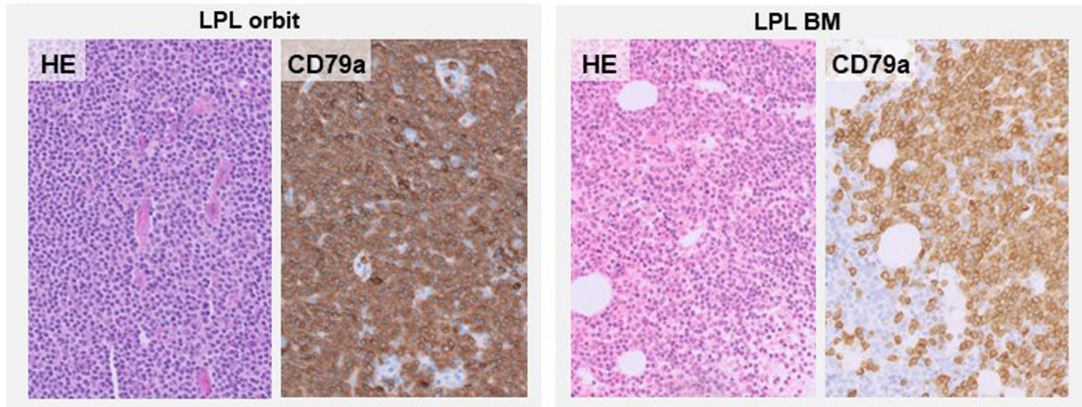


Figure 2. Temporal clonal B-cell dynamics in LPL bone marrow biopsies as revealed by NGS-based detection of IG gene rearrangements. Schematic representation of the relative distribution of 2 clonal B-cell populations (clone A, clone B) present in LPL (upper panel) as identified by next-generation sequencing (NGS)-based clonality analysis and ARResT/Interrogate bioinformatics of consecutive LPL biopsies (case 5) (lower panels), demonstrating biclonal LPL that progressed to a clonal disease over time. The clonal gene rearrangements of IGHV-IGHD-IGHJ, IGHD-IGHJ, and IGKV/Intron-KDE are shown for the LPL biopsies taken at consecutive time points (T1, T2, T3). The relative abundance of each clonotype per indicated target is depicted on the y-axis and the junction amino acid (AA) length on the x-axis. A clonotype is defined by the 5' and 3' gene annotation and the junctional nucleotide sequence of the rearrangement. AA = amino acid; BM = bone marrow; HE = hematoxylin and eosin; IG = immunoglobulin; LPL = lymphoplasmacytic lymphoma; NGS = next-generation sequencing.

A



B

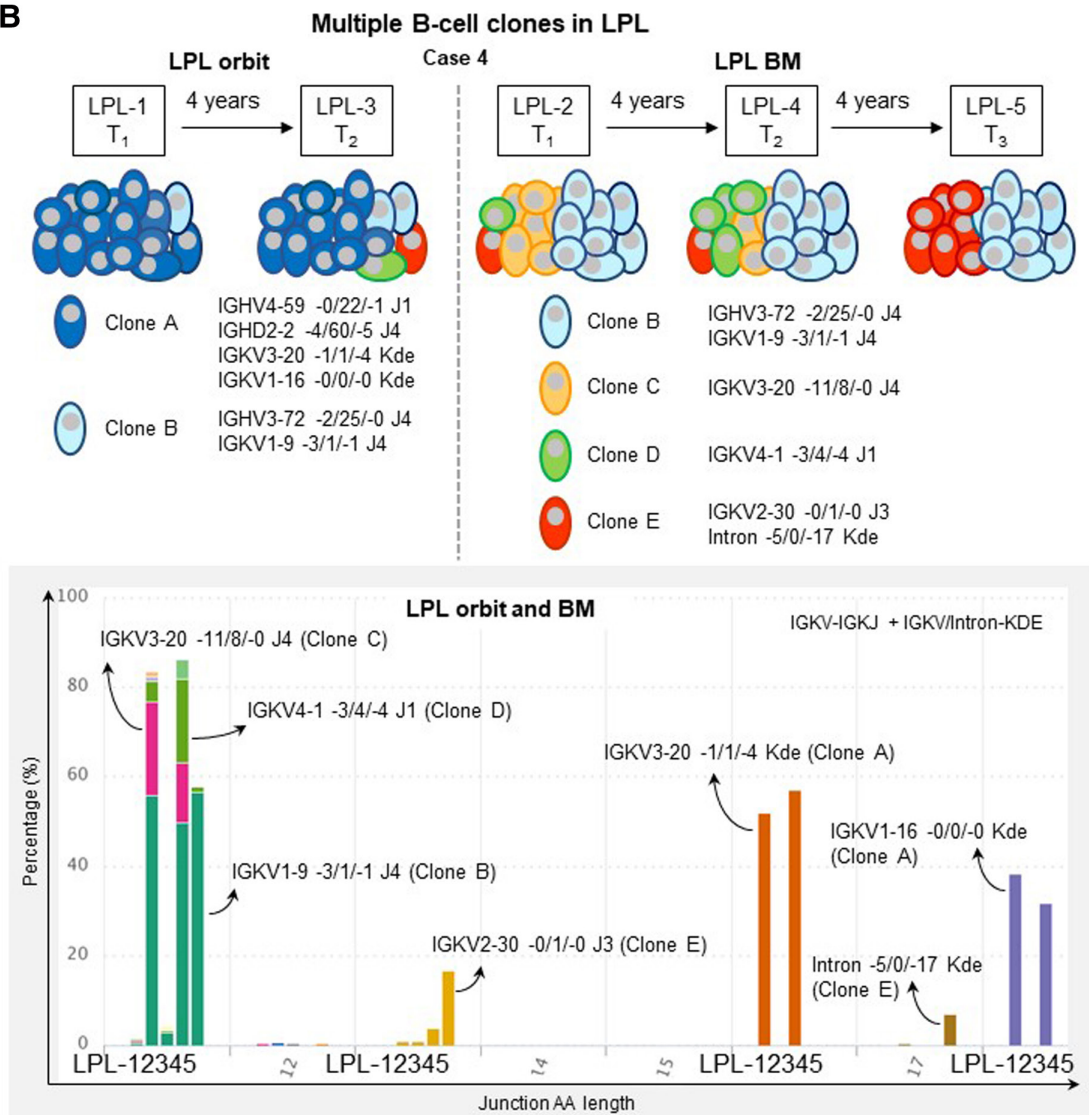


Figure 3. Temporal and spatial clonal B-cell dynamics in LPL biopsies at distinct anatomical locations. (A) Histology of 2 LPL biopsies at distinct anatomical locations (case 4), representing orbit (left panels) and bone marrow (BM) (right panels) stained with hematoxylin and eosin (H&E), or CD79a antibody. Images were taken at 200× magnification. (B) Schematic representation of the different clonal B-cell populations (clone A to clone E) and their relative frequencies present in LPL biopsies of the orbit (upper panel, left side; LPL-1 and LPL-3) or bone marrow (BM) (upper panel, right side; LPL-2, LPL-4, LPL-5) as identified by next-generation sequencing (NGS)-based clonality analysis and ARResT/Interrogate bioinformatics (case 4). Orbital and BM biopsies at T1 and T2 were taken at identical time points. The dominant clonotypes of IGK gene rearrangements (IGKV-IGKJ and IGKV/Intron-KDE) corresponding to the different B-cell clones are indicated in the lower panel. The relative abundance of each clonotype is depicted on the y-axis and the junction amino acid (AA) length on the x-axis. A clonotype is defined by the 5' and 3' gene annotation and the junctional nucleotide sequence of the rearrangement. AA = amino acid; BM = bone marrow; HE = hematoxylin and eosin; LPL = lymphoplasmacytic lymphoma; NGS = next-generation sequencing.

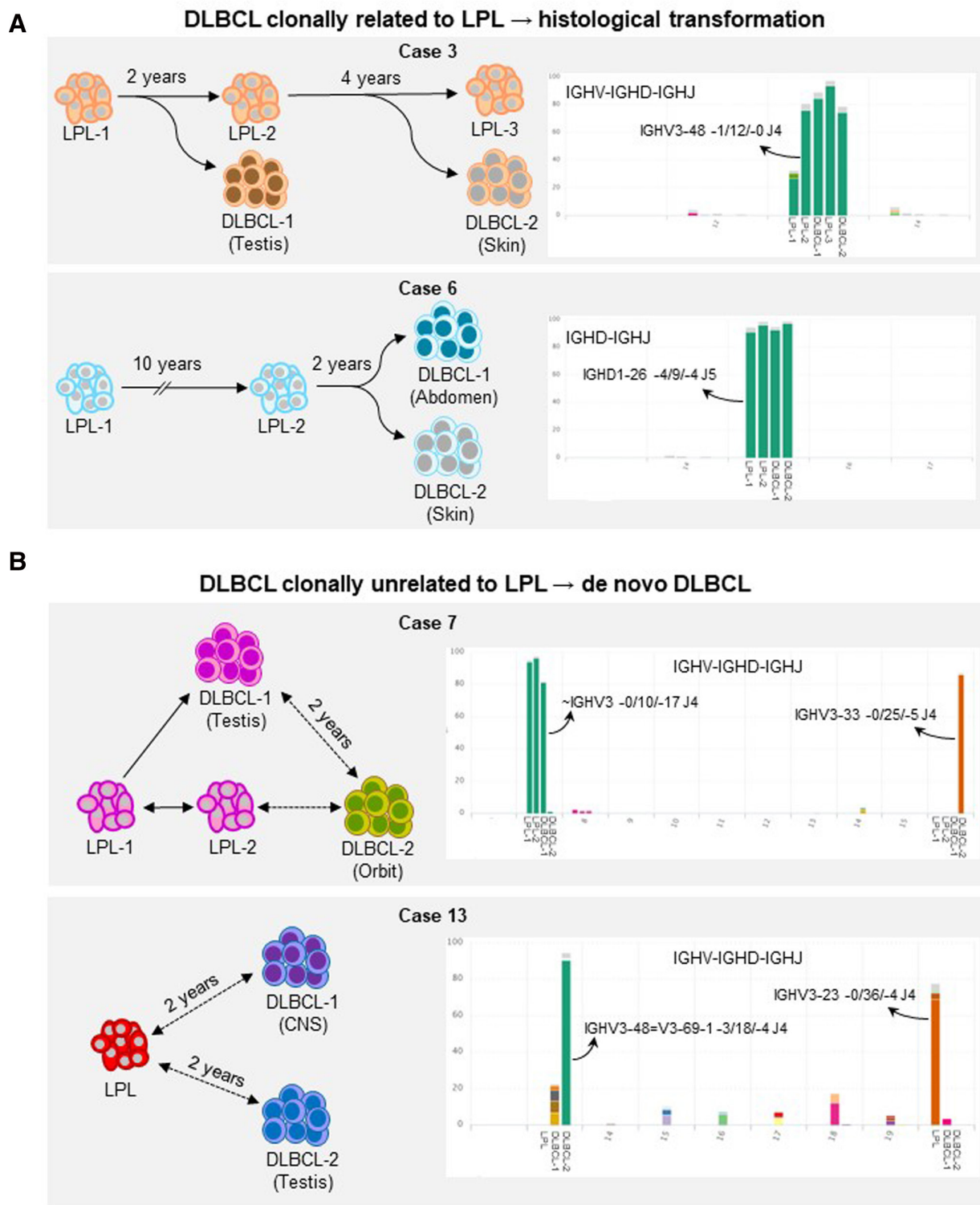


Figure 4. Establish clonal relationship of DLBCL and LPL tissue biopsies by NGS-based detection of IG gene rearrangements. (A) Next-generation sequencing (NGS)-based clonality analysis demonstrates that diffuse large B-cell lymphoma presentations are clonally related to antecedent LPL (2 representative cases: case 3 and case 6). Left panels show schematic representation of the malignant B-cell clones in the different tissue biopsies with the specific interval times indicated. Right panels depict the data from ARResT/Interrogate with the clonotype information of the predominant IGHV-IGHD-IGHJ or IGHD-IGHJ gene rearrangements, respectively. (B) NGS-based clonality assessment identifies clonally unrelated DLBCL occurrences in 2 LPL/WM patients (DLBCL-2 in case 7; DLBCL-1 and DLBCL-2 in case 13) where the dominant B-cell clones were not present in the reciprocal samples, thereby demonstrating de novo DLBCL occurrences in 2 out of 13 LPL/WM patients. Left panels show schematic representation of the B-cell clones in the different tissue biopsies with the specific interval times indicated. Right panels depict the data from ARResT/Interrogate with the clonotype information of the predominant IGHV-IGHD-IGHJ gene rearrangements. The relative abundance of each clonotype per indicated target is depicted on the y-axis and the junction amino acid (AA) length on the x-axis. A clonotype is defined by the 5' and 3' gene annotation and the junctional nucleotide sequence of the rearrangement. AA = amino acid; DLBCL = diffuse large B-cell lymphoma; IG = immunoglobulin; LPL = lymphoplasmacytic lymphoma; LPL/WM = lymphoplasmacytic lymphoma/ Waldenström macroglobulinemia; NGS = next-generation sequencing.

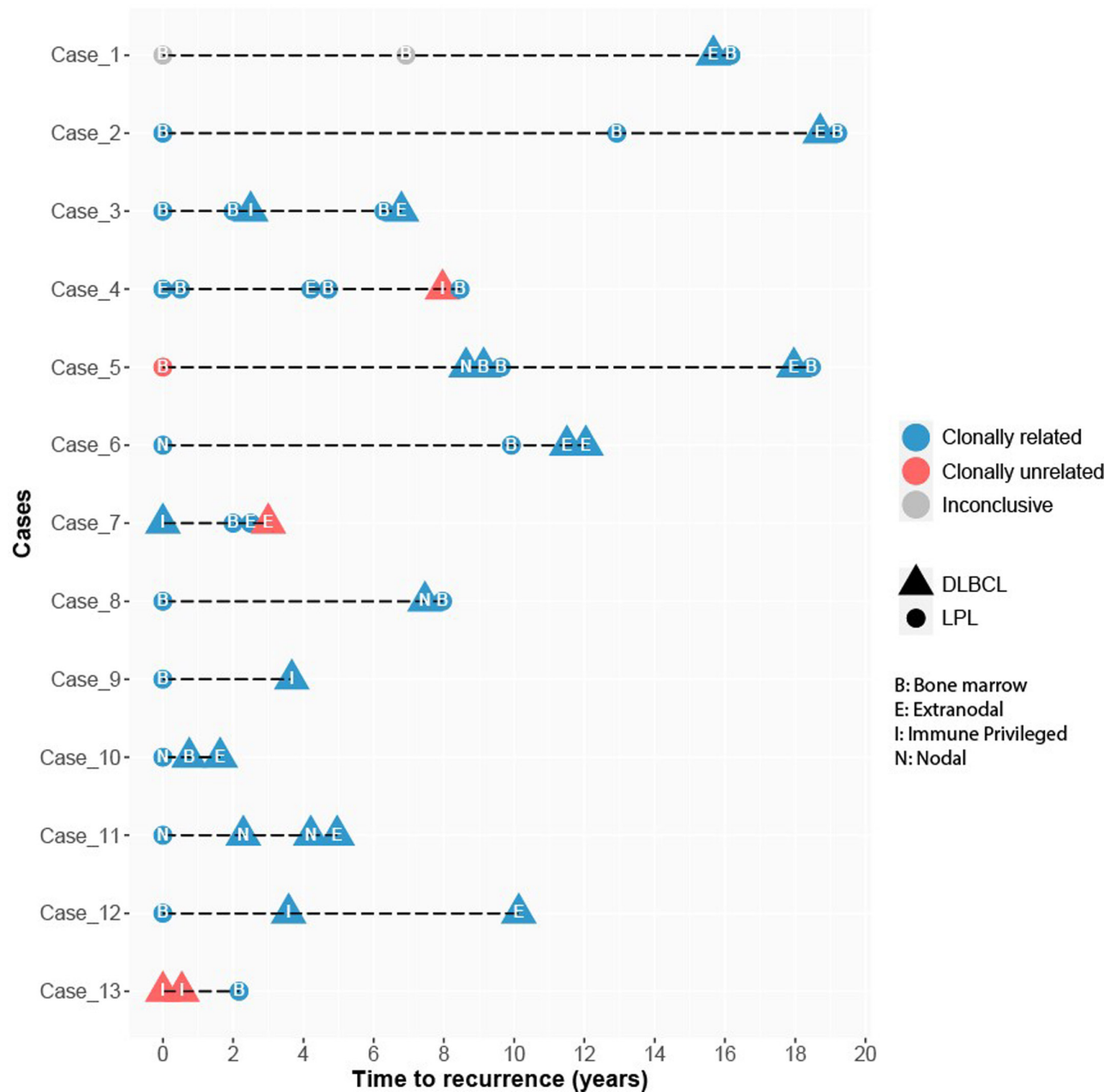


Figure 5. Summary of the clonal relationship between LPL and DLBCL presentations in LPL/WM study cohort. Clonal relationship of paired LPL and DLBCL tissue biopsies was established in 13 LPL/WM patients, in which next-generation sequencing (NGS)-based clonality assessment identified LPL- and DLBCL-specific dominant clonotype(s) in follow-up samples for each patient. Analyses revealed clonally related paired LPL-DLBCL tissue samples ($n = 10$; indicated in blue), and clonally unrelated LPL-DLBCL tissue samples ($n = 3$; indicated in red) based on the comparison of the most dominant clonotype(s) in each tissue. Some LPL samples showed inconclusive data due to inferior genomic DNA quality (indicated in gray). Circles indicate LPL biopsies and triangles DLBCL tissue biopsies. Location of biopsies are indicated: B, bone marrow; E, extranodal; I, immune privileged (central nervous system and testis); N, nodal. Per case (indicated on the y-axis), the time interval between biopsies is indicated in years on the x-axis. B = bone marrow; DLBCL = diffuse large B-cell lymphoma; E = extranodal; I = immune privileged; LPL = lymphoplasmacytic lymphoma; LPL/WM = lymphoplasmacytic lymphoma/ Waldenström macroglobulinemia; N = nodal; NGS = next-generation sequencing.

clonally unrelated DLBCL presentations were located at 2 IP sites (CNS and refractory disease in testis), which showed similar clonotypes that were distinct from LPL (Figure 4B; Suppl. Figure S2). In this patient, the DLBCL-associated clonotypes were also non-detectable in LPL using the standard IG-NGS assay. Notably, for the third patient with clonally unrelated DLBCL (case 4), the dominant B-cell clone in testicular DLBCL was detectable as a minor subclone in LPL biopsies of the orbit (Suppl. Figure S3), suggesting that this minor subclone transformed into DLBCL. Altogether, our data showed that 2 of 3

patients with clonally unrelated DLBCL displayed a de novo DLBCL (15%), while in the remaining LPL/WM patients DLBCL resulted from LPL transformation (85%).

MYD88 and CXCR4 mutation status in LPL associated with DLBCL development

Mutation status of *MYD88* and *CXCR4* harbors clinically diagnostic and therapeutic consequences for LPL/WM patients.^{34,35} To establish the presence of *MYD88* and *CXCR4*

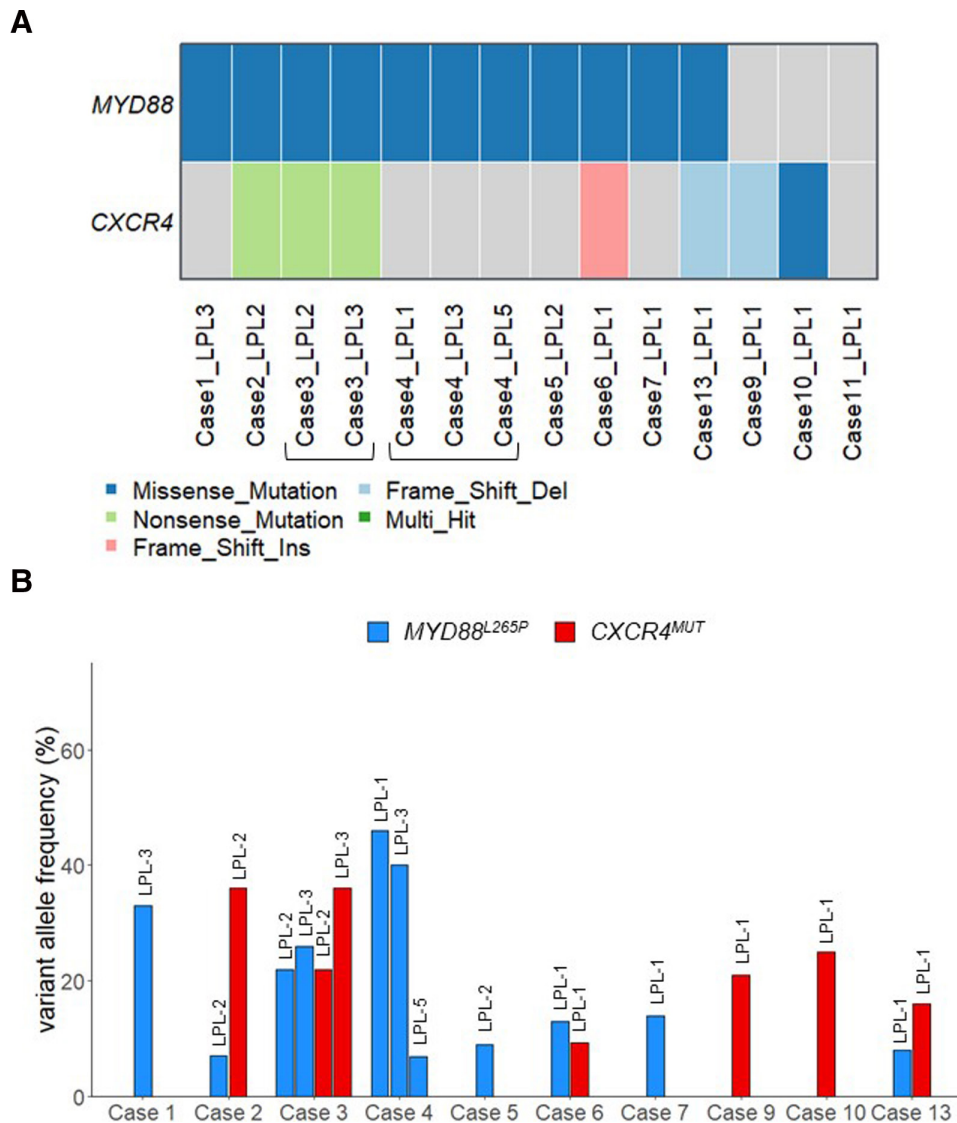


Figure 6. Overview *MYD88* and *CXCR4* status in LPL/WM study cohort. Targeted sequencing of *MYD88* and *CXCR4* in (consecutive) LPL biopsies of 11 LPL/WM patients. (A) The frequency of *MYD88*^{L265P} and *CXCR4*^{MUT} in LPL biopsies, with inclusion of the type of mutation in case of *CXCR4*^{MUT} represented by different colors. (B) Variant allele frequencies (VAF) as detected by targeted sequencing (without correction tumor percentage) of *MYD88*^{L265P} and *CXCR4*^{MUT} in LPL biopsies per case. LPL = lymphoplasmacytic lymphoma; LPL/WM = lymphoplasmacytic lymphoma/ Waldenström macroglobulinemia; VAF = variant allele frequencies.

mutations in the LPL biopsies of this study cohort, a smMIP-based approach was employed for targeted mutation analysis of 11 patients with sufficient genomic DNA available. A threshold level for the VAF of 5% was used to identify *MYD88*^{L265P} and *CXCR4*^{MUT} cases. The *MYD88*^{L265P} hotspot mutation was detected in 8/11 LPL patients (73%) with a VAF in the range of 7%-46%, indicating that 3 patients were *MYD88*^{WT} (27%; case 9, case 10, case 11) (Figure 6). Mutations targeting *CXCR4* were detected in 6/11 patients (55%) in the range of 9%-36% VAF and included 2 patients that were *MYD88*^{WT}. The *CXCR4* mutations were located at amino acid positions 322-347, involving a premature stop codon (n = 5) or missense mutation (n = 1). Cases that harbored multiple LPL clones (case 4, case 5) were *MYD88*^{L265P} and wild-type for *CXCR4* (*CXCR4*^{WT}). Clonally unrelated DLBCL occurred in patients classified as *MYD88*^{L265P} (n = 3), of which 1 patient showed a *CXCR4* mutation (case 13). In summary, LPL/WM patients with associated DLBCL showed the following genetic features: *MYD88*^{WT}*CXCR4*^{WT} (n = 1), *MYD88*^{WT}*CXCR4*^{MUT} (n = 2), *MYD88*^{L265P}*CXCR4*^{WT} (n = 4), or *MYD88*^{L265P}*CXCR4*^{MUT} subtype (n = 4).

Gene mutations contributing to LPL transformation and DLBCL development

To obtain insight into which gene mutations contributed to DLBCL development in LPL/WM patients, a total of 28 samples (n = 14 LPL; n = 14 DLBCL) of 10 patients with paired LPL-DLBCL tissue specimens were investigated (Suppl. Table S6). A substantial proportion of DLBCL biopsies in our paired study cohort eligible for mutation analysis represented IP-DLBCL (n = 5/14; 36%), or were located at other extranodal sites (n = 6/14; 43%). Therefore, a set of target genes in addition to *MYD88* and *CXCR4* was selected for mutation analysis known to be affected in IP/extranodal DLBCL (*BTG1*, *BTG2*, *CARD11*, *CD37*, *CD79B*, *PIM1*),³⁶⁻³⁸ associated with transformation in indolent lymphoma (*MYC*, *TP53*),³⁹ or acting as a cooperating tumor suppressor gene with *MYD88*^{L265P} (*TNFAIP3*).⁴⁰

In the group of LPL/WM patients with clonally related DLBCL (n = 8, including DLBCL-1 of case 7), LPL biopsies were characterized by *MYD88*^{L265P} gain-of-function mutation (n = 6), in combination with either *CXCR4* mutation (n = 2), *CXCR4* and *CD79B* mutations (n = 1), *TP53* (n = 1) or *CD37* mutation

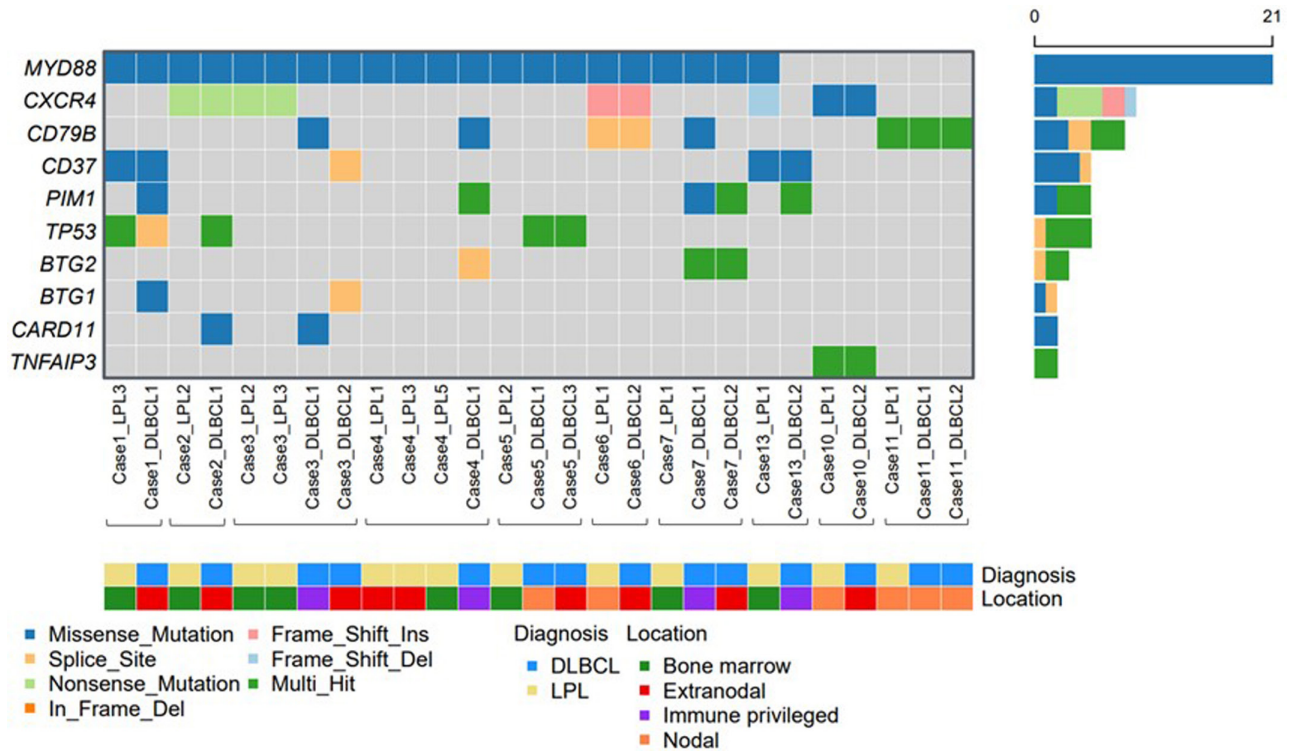


Figure 7. Distribution of gene mutations in LPL and DLBCL tissue biopsies of LPL/WM study cohort. Targeted mutation analysis in paired LPL-DLBCL tissue biopsies of 10 LPL/WM patients, which involved 1 or 2 LPL samples of each patient and available DLBCL samples for which sufficient genomic DNA was available. Case numbers are depicted in chronological order and according to *MYD88* status on the x-axis from left to right, with corresponding location of biopsy as indicated below. All identified mutations were checked for their presence in the corresponding paired LPL and DLBCL samples (Suppl. Table S6) but only depicted with a variant allele frequency (VAF) $\geq 5\%$. The type of mutation is indicated by different colors according to the legend below. Mult_hit involved 2 or more mutations per sample. DLBCL = diffuse large B-cell lymphoma; LPL = lymphoplasmacytic lymphoma; LPL/WM = lymphoplasmacytic lymphoma/ Waldenström macroglobulinemia; VAF = variant allele frequencies.

(n = 1) (Figure 7). Transformation in *MYD88^{L265P}CXCR4^{WT}* LPL (n = 3) was accompanied with recurrent acquired mutations targeting *TP53* (n = 2) and *PIM1* (n = 2), next to maintained *MYD88^{L265P}* mutation in all DLBCL tissues (n = 4). In *MYD88^{L265P}CXCR4^{MUT}* LPL transformation (n = 3), the *CXCR4* mutation was preserved after transformation in 2 patients (case 2 and case 6), but non-detectable in 2 DLBCL presentations at distinct anatomical sites of 1 patient (case 3), which displayed a pattern of divergent clonal evolution (Figure 8A). The DLBCL biopsies (n = 4) following *MYD88^{L265P}CXCR4^{MUT}* LPL transformation all maintained the *MYD88^{L265P}* mutation, with a median VAF of 69%. In these cases, LPL transformation showed acquired *CARD11* mutations (n = 2). In *MYD88^{WT}* LPL that transformed into clonally related DLBCL (n = 2), *CXCR4* and *TNFAIP3* (n = 1), or *CD79B* (n = 1) mutations were detected in both LPL and DLBCL, with no additional mutations observed in DLBCL tissues (n = 3) with our targeted gene panel. These 2 *MYD88^{WT}* cases developed through linear clonal evolution (Figure 8B). Considering all cases of clonally related LPL and DLBCL that were included in targeted mutation analysis (n = 8), LPL transformation was characterized by acquired *BTG1* (n = 2), *CARD11* (n = 2), *CD79B* (n = 2), *PIM1* (n = 2), and *TP53* (n = 2) mutations.

Patients who developed clonally unrelated DLBCL (n = 3, including DLBCL-2 of case 7) in *MYD88^{L265P}* LPL either acquired mutations in a subclone already present in LPL (case 4), or showed private de novo mutations (case 7, case 13), including *BTG2* (n = 2) and *PIM1* (n = 3) (Figure 7). One patient with de novo DLBCL also harbored a *MYD88^{L265P}* mutation in the unrelated DLBCL (DLBCL-2 case 7), while this variant was absent in the other patient with de novo DLBCL (case 13). In contrast, this patient showed a shared *CD37* mutation both

in LPL and DLBCL, suggesting a *CD37* driver mutation in the B-cell-of-origin. In summary, considering all DLBCL tissue samples, the most frequently identified individual gene mutations in DLBCL, besides *MYD88* and *CXCR4*, were represented by missense mutations in *BTG2* (n = 10) and *PIM1* (n = 18), which both reflect known target genes for SHM in DLBCL.⁴¹⁻⁴³

DISCUSSION

The clinical spectrum of LPL/WM ranges from asymptomatic precursor states to symptomatic disease, which can progress to DLBCL in a small fraction of patients. However, it is still unclear whether in all cases this progression to DLBCL results from transformation of the malignant LPL B-cell clone(s), or represents a de novo DLBCL that is clonally unrelated to LPL/WM. With the current availability of NGS-based clonality assessment, providing detailed information of (sub)clonal IG gene rearrangements, we investigated the clonal B-cell dynamics and clonal relationship of LPL and DLBCL presentations in a cohort of 13 LPL/WM patients with the EuroClonality IG-NGS assay.²⁶⁻²⁸ In addition, the *MYD88* and *CXCR4* mutational status of the LPL and DLBCL biopsies was determined by employing a targeted smMIP panel, combined with the analysis of several candidate genes associated with extranodal DLBCL development and transformation.

Patients that developed DLBCL in our study cohort, showed either stable LPL/WM disease up to ~19 years before transformation to DLBCL occurred or transformed shortly after LPL/WM diagnosis. In most cases, the identified clonotypes of the LPL neoplasm represented single B-cell clones that remained stably present in the consecutive LPL biopsies. However, in 2 patients the IG-NGS deep-sequencing approach provided evidence of >1

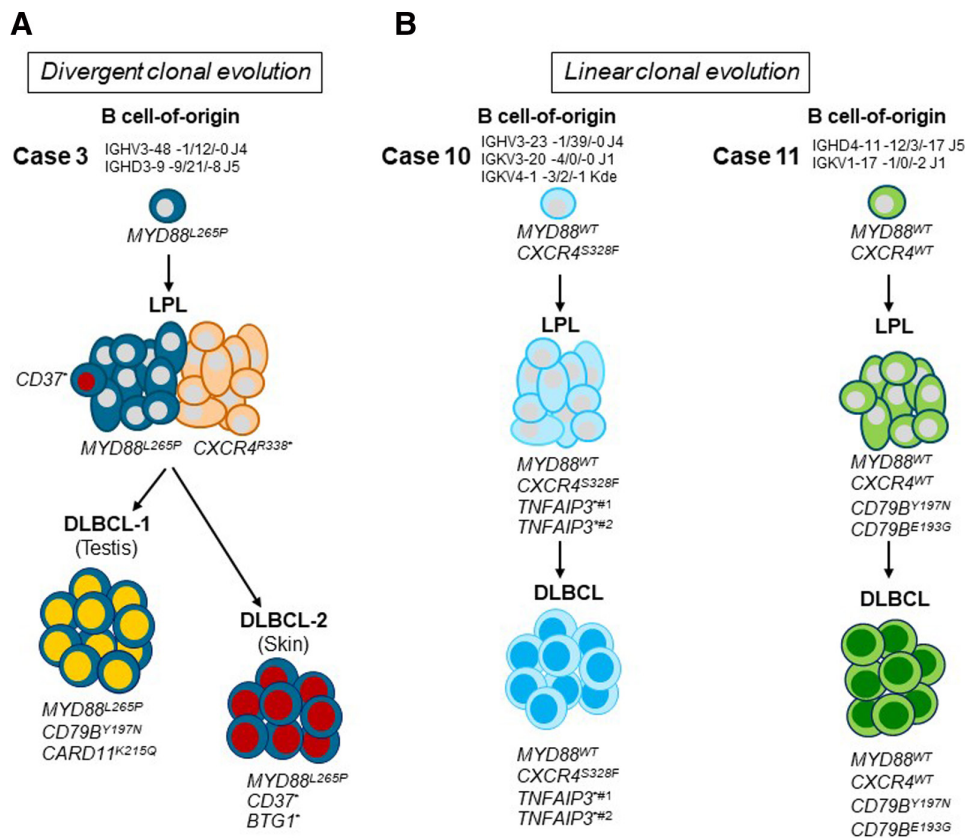


Figure 8. Integration genetic analysis indicates different clonal evolution models during histological transformation of LPL to DLBCL. Integrated analysis combining the outcome of IG-NGS clonality assessment and targeted gene mutations analysis shows that DLBCL transformation in antecedent LPL follows distinct patterns of clonal evolution. (A) Divergent clonal evolution: Two independent DLBCL neoplasms located at distinct anatomical locations (testis and skin) in 1 LPL/WM patient (case 3) developed after LPL transformation from an identical B-cell-of-origin based on identical IG gene rearrangements, but each DLBCL acquired distinct new mutations contributing to histological transformation. DLBCL-1 (testis) showed besides founder mutation *MYD88*^{L265P} also *CD79B* and *CARD11* gene mutations that were absent in DLBCL-2. On the contrary, DLBCL-2 acquired *CD37* and *BTG1* mutations, which were non-detectable in DLBCL-1. The tumor clone of DLBCL-2 was present in the antecedent LPL as a minor subclone by detecting the same *CD37* mutation at a very low variant allele frequency in LPL (1.3%; see Suppl. Table S6). (B) Linear clonal evolution: transformation of either *MYD88*^{WT}*CXCR4*^{MUT} (case 10) or *MYD88*^{WT}*CXCR4*^{WT} (case 11) LPL into DLBCL is characterized by the acquisition of at least 2 *TNFAIP3* and 2 *CD79B* gene mutations, respectively. Superscript * indicates a loss-of-function alteration (aberrant splicing, missense mutation leading to stop codon). DLBCL = diffuse large B-cell lymphoma; LPL = lymphoplasmacytic lymphoma; LPL/WM = lymphoplasmacytic lymphoma/ Waldenström macroglobulinemia.

malignant B-cell clone in LPL, showing biclonal LPL as well as dynamic clonal heterogeneity represented possibly by at least 3 malignant B-cell clones in LPL at distinct anatomical sites. Our findings of detecting multiple B-cell clones in LPL confirm the observations of others performing clonotypic V(D)J analysis in LPL/WM patients.¹²⁻¹⁴ The presence of clonal diversity represented by unrelated B-cell clones has been observed in several other B-cell malignancies, including classic Hodgkin lymphoma,²⁵ multiple myeloma,⁴⁴ and chronic lymphocytic leukemia.⁴⁵

To establish the clonal relationship of the consecutive LPL and DLBCL presentations in our LPL/WM cohort, the clonotypes of the malignant B-cell clones identified in the corresponding B-cell lymphomas were compared to each other. In 11 out of 13 patients, identical IG gene rearrangements were detected in LPL and (one of the) DLBCL tissue samples (including DLBCL-1 of case 7), arguing that these DLBCL occurrences represented the actual transformation of the antecedent LPL. Integrating clonality and mutation analysis indicated that LPL transformation occurred through different patterns of clonal evolution, including linear and divergent evolution. The process of transformation resulting in DLBCL development involved the preservation of critical driver mutations, like *MYD88*^{L265P}, as well as the acquisition of additional gene mutations driving DLBCL development. Many of the DLBCL occurrences represented extranodal DLBCL, which can be explained by the predilection of *MYD88*^{L265P} at

this anatomical site.⁴⁶ In our study, *BTG1*, *BTG2*, *CARD11*, *TP53*, *CD79B* and *PIM1* mutations were recurrently acquired in DLBCL, where *BTG1*, *BTG2*, *CARD11* and *PIM1* mutations were exclusively present in DLBCL upon transformation.

Antiproliferated tumor suppressors of the BTG/TOB protein family that play a role in multiple cellular processes, including transcription regulation, DNA repair, cell division, and messenger RNA stability.⁴⁷ Inactivating *BTG1* mutations promote lymphomagenesis by dysregulating several key processes leading to enhanced oncogenic fitness and cell migration.^{48,49} The mutations we identified in *CARD11* were located within the coiled-coil domain of scaffold protein *CARD11* (K215Q and L341V), a region that is often mutated in DLBCL.⁵⁰ *CARD11* is a crucial adaptor protein acting downstream of antigen receptor signaling, regulating signaling pathways involved in immune function and cell survival.⁵¹ Whether these specific mutations identified in our study represent oncogenic gain-of-function mutations of *CARD11* activating downstream NF- κ B signaling remains to be investigated. The exclusive role of *PIM1* in LPL transformation has also been confirmed in a previous whole-exome sequencing study of DLBCL with antecedent LPL.⁵² *PIM1* represents a serine/threonine kinase that acts in several signaling pathways regulating cell survival, metabolism, and cell proliferation.^{53,54} Since *PIM1* is a common off-target of activation-induced cytidine deaminase-mediated

SHM in DLBCL, the role of these mutations in enhancing the oncogenic potential of PIM1 remains to be established.

Besides the DLBCL occurrences that developed through LPL transformation, in 3 out of 13 LPL/WM patients (23%) clonally unrelated lymphomas were identified in one of the DLBCL biopsies, demonstrated by the presence of different dominant clonotypes for 2 or more IG targets. These involved a total of 4 DLBCL presentations, which included 3 IP-DLBCL located at CNS (n = 1) and testis (n = 2), and 1 orbital lymphoma. Primary CNS and testicular large B-cell lymphoma are characterized by a high frequency of MYD88 mutations (60%–80% of patients),^{55–59} which involve a spectrum of MYD88 mutations, but MYD88^{L265P} hotspot mutation represents the most dominant one. On the other hand, ocular adnexal large B-cell lymphoma harbors MYD88 mutations in only ~30% of the cases.⁶⁰ In our study, in 2 patients biopsies of clonally unrelated LPL and DLBCL located at testis and orbit (cases 4 and 7) were MYD88^{L265P}, suggesting that the LPL and DLBCL originated from a common MYD88^{L265P} ancestor cell before IG V(D)J recombination took place through divergent (branching) evolution, or developed through independent clonal evolution with a second MYD88^{L265P} mutation event. These 2 cases represent only a very small group of patients, and further studies in larger cohorts of LPL/WM patients with DLBCL are required to determine how often these events occur. Two IP-DLBCL presentations in the third patient (case 13) were MYD88^{WT}, while the LPL showed the MYD88^{L265P} mutations. Instead, these IP-DLBCL harbored CD37 and PIM1 mutations, which likely contribute to B-cell survival signaling at these IP sites.^{38,61} Indeed, previous studies identified CD37 mutations exclusively present in IP-DLBCL (23%) and not in nodal DLBCL,³⁸ indicating a predilection for CD37 inactivation at these IP sites.

The MYD88^{L265P} hotspot mutation is a major driver of LPL/WM, but clearly not sufficient for LPL/WM development as also demonstrated in mouse models.^{62,63} In this study, MYD88^{L265P} was present in 8 out of 11 patients (73%) and was detected in both LPL and DLBCL of all transformed cases. Conversely, MYD88^{WT} was present in almost one-quarter of patients in our cohort, which is higher compared to regular LPL/WM (<5%), and is in line with previous findings where MYD88^{WT} has been associated with DLBCL occurrences.¹⁹ Furthermore, CXCR4 mutations were identified in LPL biopsies of 6 out of 11 patients (55%), and correspond to the more aggressive disease of CXCR4^{MUT} subtype.^{22,23} Notably, LPL biopsies in 2 patients harbored CXCR4 mutations without MYD88^{L265P} hotspot mutation, which has been shown to be quite rare.³⁴ Besides these 2 well-established hallmarks of LPL/WM disease, CD79B, TNFAIP3, and CD37 mutations were also recurrently present in LPL biopsies, contributing to the genomic landscape of LPL/WM.^{21,34} Furthermore, we detected in 1 MYD88^{L265P} LPL biopsy TP53 mutations, which are associated with adverse outcome in LPL/WM patients.^{64–66}

In conclusion, our data demonstrated temporal and spatial clonal dynamics in LPL patients that developed DLBCL, which occurred through transformation in the majority of LPL/WM patients accompanied by acquired mutations targeting BTG1, BTG2, CARD11, CD79B, PIM1, and TP53. However, in approximately 25% of the cases, clonally unrelated DLBCL was observed, which involved de novo DLBCL in 15% of the patients, suggesting that LPL/WM patients with associated DLBCL may harbor an increased risk of second primary lymphoma.

ACKNOWLEDGMENTS

We would like to acknowledge the EuroClonality-NGS Working Group for support with IG-NGS protocols and ArresT/Interrogate bioinformatics pipeline. We would like to thank Karin Beunen for collecting clinical data at Rijnstate Hospital; Anouk Smits and Teun Jakobs for DNA isolation and data analysis, and staff from the Department of Human Genetics for preparing the next-generation sequence runs.

AUTHOR CONTRIBUTIONS

BS, JHJMvK, and MvdB conceived the project. MRB and CBI carried out the experimental research. MRB, DAGvB, ABvS, KMH, MvdB, PJTAG, and BS analyzed the data. MRB, EH, EvdS, SC, WBCS, and MvdB collected diagnostic materials and clinical data. MvdB and JHJMvK performed pathology review. MRB and BS wrote the article. All authors have read and approved the article.

DISCLOSURES

The authors have no conflicts of interest to disclose.

SOURCES OF FUNDING

This work was funded by Hematon (OfH2022-1) and the Dutch Cancer Society (KWF-11137). ABvS is supported by the Netherlands Organization for Scientific Research (NWO) (ZonMW project 09120012010023), Dutch Cancer Society (projects 12949 and 14726), and European Research Council (Consolidator Grant 724281 and Proof-of-Concept Grant 101112687).

REFERENCES

- Vitolo U, Ferreri AJ, Montoto S. Lymphoplasmacytic lymphoma-Waldenstrom's macroglobulinemia. *Crit Rev Oncol Hematol*. 2008;67:172–185.
- Askari E, Rodriguez S, Garcia-Sanz R. Waldenstrom's macroglobulinemia: an exploration into the pathology and diagnosis of a complex B-cell malignancy. *J Blood Med*. 2021;12:795–807.
- Lin P, Mansoor A, Bueso-Ramos C, et al. Diffuse large B-cell lymphoma occurring in patients with lymphoplasmacytic lymphoma/Waldenstrom macroglobulinemia clinicopathologic features of 12 cases. *Am J Clin Pathol*. 2003;120:246–253.
- Leleu X, Soumerai J, Roccaro A, et al. Increased incidence of transformation and myelodysplasia/acute leukemia in patients with Waldenstrom macroglobulinemia treated with nucleoside analogs. *J Clin Oncol*. 2009;27:250–255.
- Castillo JJ, Gustine J, Meid K, et al. Histological transformation to diffuse large B-cell lymphoma in patients with Waldenstrom macroglobulinemia. *Am J Hematol*. 2016;91:1032–1035.
- Durot E, Tomowiak C, Michallet AS, et al. Transformed Waldenstrom macroglobulinemia: clinical presentation and outcome a multi-institutional retrospective study of 77 cases from the French Innovative Leukemia Organization (FILO). *Br J Haematol*. 2017;179:439–448.
- Talaulikar D, Biscoe A, Lim JH, et al. Genetic analysis of diffuse large B-cell lymphoma occurring in cases with antecedent Waldenstrom macroglobulinemia reveals different patterns of clonal evolution. *Br J Haematol*. 2019;185:767–770.
- Boiza-Sanchez M, Manso R, Balague O, et al. Lymphoplasmacytic lymphoma associated with diffuse large B-cell lymphoma: progression or divergent evolution? *PLoS One*. 2020;15:e0241634.
- Shimizu S, Tamagawa Y, Kojima H, et al. Simultaneous development of lymphoplasmacytic lymphoma and diffuse large B-cell lymphoma--analyses of the clonal relatedness by sequencing CDR3 in immunoglobulin heavy chain genes. *Eur J Haematol*. 2003;70:119–124.
- Tojo K, Hattori T, Ito T, et al. Multiple brain tumors of diffuse large B cell lymphoma in a patient with Waldenstrom's macroglobulinemia/lymphoplasmacytic lymphoma: PCR and DNA sequence analysis show evidence of differences in clonality of the two B cell malignancies. *Intern Med*. 2004;43:990–996.
- Owen RG, Bynoe AG, Varghese A, et al. Heterogeneity of histological transformation events in Waldenstrom's macroglobulinemia (WM) and related disorders. *Clin Lymphoma Myeloma Leuk*. 2011;11:176–179.
- Kriangkum J, Taylor BJ, Treon SP, et al. Molecular characterization of Waldenstrom's macroglobulinemia reveals frequent occurrence of two B-cell clones having distinct IgH VDJ sequences. *Clin Cancer Res*. 2007;13:2005–2013.
- Kirshner J, Thulien KJ, Kriangkum J, et al. In a patient with biconal Waldenstrom macroglobulinemia only one clone expands in three-dimensional culture and includes putative cancer stem cells. *Leuk Lymphoma*. 2011;52:285–289.
- Wang W, Ding Y, Campbell A, et al. Biconal presentation of lymphoplasmacytic lymphoma/Waldenstrom macroglobulinemia. *Pathology (Phila)*. 2019;51:340–343.
- Treon SP, Xu L, Yang G, et al. MYD88 L265P somatic mutation in Waldenstrom's macroglobulinemia. *N Engl J Med*. 2012;367:826–833.
- Jimenez C, Sebastian E, Chillon MC, et al. MYD88 L265P is a marker highly characteristic of, but not restricted to, Waldenstrom's macroglobulinemia. *Leukemia*. 2013;27:1722–1728.

17. Poulain S, Roumier C, Decambion A, et al. MYD88 L265P mutation in Waldenstrom macroglobulinemia. *Blood*. 2013;121:4504–4511.
18. Varettoni M, Arcaini L, Zibellini S, et al. Prevalence and clinical significance of the MYD88 (L265P) somatic mutation in Waldenstrom's macroglobulinemia and related lymphoid neoplasms. *Blood*. 2013;121:2522–2528.
19. Treon SP, Gustine J, Xu L, et al. MYD88 wild-type Waldenstrom macroglobulinemia: differential diagnosis, risk of histological transformation, and overall survival. *Br J Haematol*. 2018;180:374–380.
20. Zanwar S, Abeykoon JP, Durot E, et al. Impact of MYD88(L265P) mutation status on histological transformation of Waldenstrom macroglobulinemia. *Am J Hematol*. 2020;95:274–281.
21. Hunter ZR, Xu L, Yang G, et al. The genomic landscape of Waldenstrom macroglobulinemia is characterized by highly recurring MYD88 and WHIM-like CXCR4 mutations, and small somatic deletions associated with B-cell lymphomagenesis. *Blood*. 2014;123:1637–1646.
22. Treon SP, Cao Y, Xu L, et al. Somatic mutations in MYD88 and CXCR4 are determinants of clinical presentation and overall survival in Waldenstrom macroglobulinemia. *Blood*. 2014;123:2791–2796.
23. Roccaro AM, Sacco A, Jimenez C, et al. C1013G/CXCR4 acts as a driver mutation of tumor progression and modulator of drug resistance in lymphoplasmacytic lymphoma. *Blood*. 2014;123:4120–4131.
24. Varettoni M, Zibellini S, DeFrancesco I, et al. Pattern of somatic mutations in patients with Waldenstrom macroglobulinemia or IgM monoclonal gammopathy of undetermined significance. *Haematologica*. 2017;102:2077–2085.
25. van Bladel DAG, van den Brand M, Rijntjes J, et al. Clonality assessment and detection of clonal diversity in classic Hodgkin lymphoma by next-generation sequencing of immunoglobulin gene rearrangements. *Mod Pathol*. 2022;35:757–766.
26. Scheijen B, Meijers RWJ, Rijntjes J, et al. Next-generation sequencing of immunoglobulin gene rearrangements for clonality assessment: a technical feasibility study by EuroClonality-NGS. *Leukemia*. 2019;33:2227–2240.
27. van den Brand M, Rijntjes J, Mobs M, et al. Next-generation sequencing-based clonality assessment of Ig gene rearrangements: a multicenter validation study by EuroClonality-NGS. *J Mol Diagn*. 2021;23:1105–1115.
28. van Bladel DAG, van der Last-Kempkes JLM, Scheijen B, et al. Next-generation sequencing-based clonality detection of immunoglobulin gene rearrangements in B-cell lymphoma. *Methods Mol Biol*. 2022;2453:7–42.
29. Berendsen MR, Bladel D, Hesius E, et al. Detection of second primary lymphoma in late diffuse large B-cell lymphoma recurrences. *Mod Pathol*. 2023;36:100119.
30. Eijkelenboom A, Kamping EJ, Kastner-van Raaij AW, et al. Reliable next-generation sequencing of formalin-fixed, paraffin-embedded tissue using single molecule tags. *J Mol Diagn*. 2016;18:851–863.
31. Langerak AW, Groenen PJ, Bruggemann M, et al. EuroClonality/BIOMED-2 guidelines for interpretation and reporting of Ig/TCR clonality testing in suspected lymphoproliferations. *Leukemia*. 2012;26:2159–2171.
32. Hartmann S, Helling A, Doring C, et al. Clonality testing of malignant lymphomas with the BIOMED-2 primers in a large cohort of 1969 primary and consultant biopsies. *Pathol Res Pract*. 2013;209:495–502.
33. Lu C, He Q, Zhu W, et al. The value of detecting immunoglobulin gene rearrangements in the diagnosis of B-cell lymphoma. *Oncotarget*. 2017;8:77009–77019.
34. Treon SP, Xu L, Guerrero ML, et al. Genomic landscape of Waldenstrom macroglobulinemia and its impact on treatment strategies. *J Clin Oncol*. 2020;38:1198–1208.
35. Kaiser LM, Hunter ZR, Treon SP, et al. CXCR4 in Waldenstrom's macroglobulinemia: chances and challenges. *Leukemia*. 2021;35:333–345.
36. Chapuy B, Stewart C, Dunford AJ, et al. Molecular subtypes of diffuse large B cell lymphoma are associated with distinct pathogenic mechanisms and outcomes. *Nat Med*. 2018;24:679–690.
37. Schmitz R, Wright GW, Huang DW, et al. Genetics and pathogenesis of diffuse large B-cell lymphoma. *N Engl J Med*. 2018;378:1396–1407.
38. Elfrink S, de Winde CM, van den Brand M, et al. High frequency of inactivating tetraspanin C D37 mutations in diffuse large B-cell lymphoma at immune-privileged sites. *Blood*. 2019;134:946–950.
39. Pasqualucci L, Khiabani H, Fangazio M, et al. Genetics of follicular lymphoma transformation. *Cell Rep*. 2014;6:130–140.
40. Wenzl K, Manske MK, Sarangi V, et al. Loss of TNFAIP3 enhances MYD88(L265P)-driven signaling in non-Hodgkin lymphoma. *Blood Cancer J*. 2018;8:97.
41. Pasqualucci L, Neumeister P, Goossens T, et al. Hypermutation of multiple proto-oncogenes in B-cell diffuse large-cell lymphomas. *Nature*. 2001;412:341–346.
42. Khodabakhshi AH, Morin RD, Fejes AP, et al. Recurrent targets of aberrant somatic hypermutation in lymphoma. *Oncotarget*. 2012;3:1308–1319.
43. Alkodsai A, Cervera A, Zhang K, et al. Distinct subtypes of diffuse large B-cell lymphoma defined by hypermutated genes. *Leukemia*. 2019;33:2662–2672.
44. Kriangkum J, Motz SN, Debes Marun CS, et al. Frequent occurrence of highly expanded but unrelated B-cell clones in patients with multiple myeloma. *PLoS One*. 2013;8:e64927.
45. Kriangkum J, Motz SN, Mack T, et al. Single-cell analysis and next-generation immunosequencing show that multiple clones persist in patients with chronic lymphocytic leukemia. *PLoS One*. 2015;10:e0137232.
46. King RL, Goodlad JR, Calaminici M, et al. Lymphomas arising in immune-privileged sites: insights into biology, diagnosis, and pathogenesis. *Virchows Arch*. 2020;476:647–665.
47. Yuniati L, Scheijen B, van der Meer LT, et al. Tumor suppressors BTG1 and BTG2: beyond growth control. *J Cell Physiol*. 2019;234:5379–5389.
48. Delage L, Lambert M, Bardel E, et al. BTG1 inactivation drives lymphomagenesis and promotes lymphoma dissemination through activation of BCAR1. *Blood*. 2023;141:1209–1220.
49. Mlynarczyk C, Teater M, Pae J, et al. BTG1 mutation yields supercompetitive B cells primed for malignant transformation. *Science*. 2023;379:eabj7412.
50. Lenz G, Davis RE, Ngo VN, et al. Oncogenic CARD11 mutations in human diffuse large B cell lymphoma. *Science*. 2008;319:1676–1679.
51. Bedsaul JR, Carter NM, Deibel KE, et al. Mechanisms of regulated and dysregulated CARD11 signaling in adaptive immunity and disease. *Front Immunol*. 2018;9:2105.
52. Jimenez C, Alonso-Alvarez S, Alcoceba M, et al. From Waldenstrom's macroglobulinemia to aggressive diffuse large B-cell lymphoma: a whole-exome analysis of abnormalities leading to transformation. *Blood Cancer J*. 2017;7:e591.
53. Zhang H, Lu Y, Zhang T, et al. PIM1 genetic alterations associated with distinct molecular profiles, phenotypes and drug responses in diffuse large B-cell lymphoma. *Clin Transl Med*. 2022;12:e808.
54. Bellon M, Nicot C. Targeting PIM kinases in hematological cancers: molecular and clinical review. *Mol Cancer*. 2023;22:18.
55. Montesinos-Rongen M, Godlewska E, Brunn A, et al. Activating L265P mutations of the MYD88 gene are common in primary central nervous system lymphoma. *Acta Neuropathol*. 2011;122:791–792.
56. Bodor C, Alpar D, Marosvari D, et al. Molecular subtypes and genomic profile of primary central nervous system lymphoma. *J Neuropathol Exp Neurol*. 2020;79:176–183.
57. Radke J, Ishaque N, Koll R, et al. The genomic and transcriptional landscape of primary central nervous system lymphoma. *Nat Commun*. 2022;13:2558.
58. Chapuy B, Roemer MG, Stewart C, et al. Targetable genetic features of primary testicular and primary central nervous system lymphomas. *Blood*. 2016;127:869–881.
59. Kraan W, van Keimpema M, Horlings HM, et al. High prevalence of oncogenic MYD88 and CD79B mutations in primary testicular diffuse large B-cell lymphoma. *Leukemia*. 2014;28:719–720.
60. Kirkegaard MK, Minderman M, Sjo LD, et al. Prevalence and prognostic value of MYD88 and CD79B mutations in ocular adnexal large B-cell lymphoma: a reclassification of ocular adnexal large B-cell lymphoma. *Br J Ophthalmol*. 2023;107:576–581.
61. Fukumura K, Kawazu M, Kojima S, et al. Genomic characterization of primary central nervous system lymphoma. *Acta Neuropathol*. 2016;131:865–875.
62. Sewastianik T, Guerrero ML, Adler K, et al. Human MYD88L265P is insufficient by itself to drive neoplastic transformation in mature mouse B cells. *Blood Adv*. 2019;3:3360–3374.
63. Ouk C, Roland L, Gachard N, et al. Continuous MYD88 activation is associated with expansion and then transformation of IgM differentiating plasma cells. *Front Immunol*. 2021;12:641692.
64. Poulain S, Roumier C, Bertrand E, et al. TP53 Mutation and its prognostic significance in Waldenstrom's macroglobulinemia. *Clin Cancer Res*. 2017;23:6325–6335.
65. Gustine JN, Tsakmaklis N, Demos MG, et al. TP53 mutations are associated with mutated MYD88 and CXCR4, and confer an adverse outcome in Waldenstrom macroglobulinemia. *Br J Haematol*. 2019;184:242–245.
66. Wang Y, Gali VL, Xu-Monette ZY, et al. Molecular and genetic biomarkers implemented from next-generation sequencing provide treatment insights in clinical practice for Waldenstrom macroglobulinemia. *Neoplasia*. 2021;23:361–374.